ACS Photonics

Article

pubs.acs.org/journal/apchd5

Tunable Plasmon–Phonon Polaritons in Layered Graphene–Hexagonal Boron Nitride Heterostructures

Yichen Jia,[†] Huan Zhao,[‡] Qiushi Guo,[†] Xiaomu Wang,[†] Han Wang,[‡] and Fengnian Xia*[,†]

[†]Department of Electrical Engineering, Yale University, 15 Prospect Street, New Haven, Connecticut 06511, United States

[‡]Ming Hsieh Department of Electrical Engineering, University of Southern California, 3737 Watt Way, Los Angeles, California 90089, United States

Supporting Information

ABSTRACT: We use infrared spectroscopy to explore the hybridization of graphene plasmons and hexagonal boron nitride (hBN) phonons in their heterostructures with different compositions. We show that the degree of plasmon–phonon hybridization and the slowing of the light group velocity within the infrared transparency window due to the plasmon–phonon destructive interference are dominated by hBN phonon oscillating strength, which can be tuned by varying the hBN thickness in a layer-by-layer manner. However, the plasmon oscillating strength in metallic graphene governs the magnitude of infrared extinction, which exceeds 6% at around 7 μm in a graphene/hBN/graphene heterostructure due to the strong plasmon dipole–dipole coupling. Our work demonstrates that the infrared optical responses of graphene–hBN heterostructures can be engineered by controlling the coupling strength of plasmon–phonon hybridization and the overall plasmon oscillating strength simultaneously, thus opening the avenue for the light manipulation and detection in the mid-infrared regime based on such layered heterostructures.

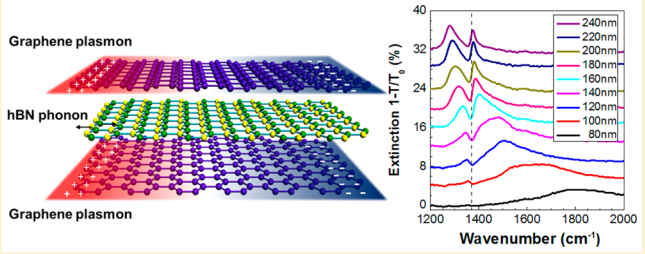

KEYWORDS: *infrared spectroscopy, graphene, hBN, plasmon–phonon polariton, slow light*

Graphene plasmon has recently attracted widespread attention due to its tunability,[1−10] potentially low loss,[11,12] and possible applications in infrared light manipulation and detection.[13−20] The graphene plasmon primarily occupies the wavelength range from terahertz to mid-infrared (~4 μm, or 2500 cm^{-1}), due to its relatively low carrier density compared with that of traditional plasmonic materials such as silver and gold.[15,21−24] Interestingly, an infrared-active phonon mode in another dielectric two-dimensional (2D) material, hexagonal boron nitride (hBN), also resides in mid-infrared at around 1370 cm^{-1}.[25,26] Recently, Brar et al. demonstrated that the coupling of plasmon in monolayer graphene and phonon in monolayer hBN leads to hybridized plasmon–phonon modes.[27] In addition, the continuous control of hyperbolic phonon polaritons in hBN slabs by graphene plasmons was also systematically studied by Dai et al.[28] In this work, we engineer the infrared optical responses of graphene–hBN heterostructures by controlling the plasmon and phonon oscillating strengths, respectively, in a layer-by-layer manner. Both graphene and hBN samples were grown by chemical vapor deposition (CVD) on copper and transferred to a highly resistive silicon wafer with 90 nm of silicon oxide on top, in sequence, to form the desirable heterostructures.[29,30] Detailed fabrication processes are presented in Supporting Information. We pattern the heterostructures into nanoribbons for direct excitation of plasmon–phonon polaritons. The schematic of our experiment is shown in Figure 1a. A Fourier transform infrared spectroscopy (FTIR) spectrometer integrated with a microscope is utilized to determine the spectral response of the graphene–hBN heterostructures. The polarization is controlled through a zinc selenide holographic wire grid polarizer

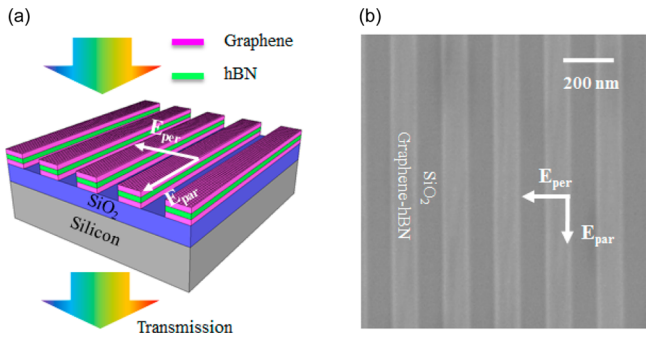

Figure 1. Schematic of the experiment. (a) Mid-infrared transmission measurement scheme for graphene/hBN/graphene heterostructure nanoribbons. The excitation light is broadband. E_{per} and E_{par} denote light polarizations perpendicular and parallel to the ribbons, respectively. (b) SEM image of a typical array of graphene–hBN heterostructure nanoribbons. The physical width of the ribbons shown is 100 nm.

Received: March 5, 2015
Published: June 19, 2015

DOI: 10.1021/acsphotonics.5b00099
ACS Photonics 2015, 2, 907−912

mounted on a rotatable adaptor. Figure 1b shows a scanning electron microscope (SEM) image of a patterned graphene−hBN nanoribbon array. We use transmission extinction, $1 - T/T_0$,[31] to characterize the infrared optical responses of these heterostructure nanoribbon arrays, where T is the transmission of the light through the ribbon array and the substrate and T_0 is the transmission through the bare substrate.

RESULTS

Before the characterization of graphene−hBN heterostructures, we first studied the infrared response of mono- and few-layer hBN nanoribbons to determine the layer dependence of the oscillating strength, which is defined as the average power per unit area consumed by the phonon oscillation in the classical oscillator model (see Supporting Information for details). The phonon dispersion of few-layer hBN differs drastically from that of bulk hBN.[32] Figure 2a illustrates the mid-infrared extinction spectra of mono-, bi-, and trilayer hBN nanoribbon arrays with an effective ribbon width W_e = 120 nm. The effective ribbon width W_e here is defined as $W_e = W - W_0$, in which W is the ribbon's physical width and W_0 (20 nm in this work) accounts for defects and edge chemistry caused by the fabrication process[11,33] (see Supporting Information for details). In the monolayer case, when the polarization of the incident light is parallel to the ribbons, the peak centers at 1370 cm^{-1}, which represents the degenerate Γ point phonon mode residing in the upper Reststrahlen band.[34] When the incident polarization is perpendicular to the ribbons, the phonon peak position upshifts to 1373 cm^{-1}. Such a blue shift is larger and reaches 1377 and 1379 cm^{-1} in bilayer and trilayer hBN nanoribbons, respectively.

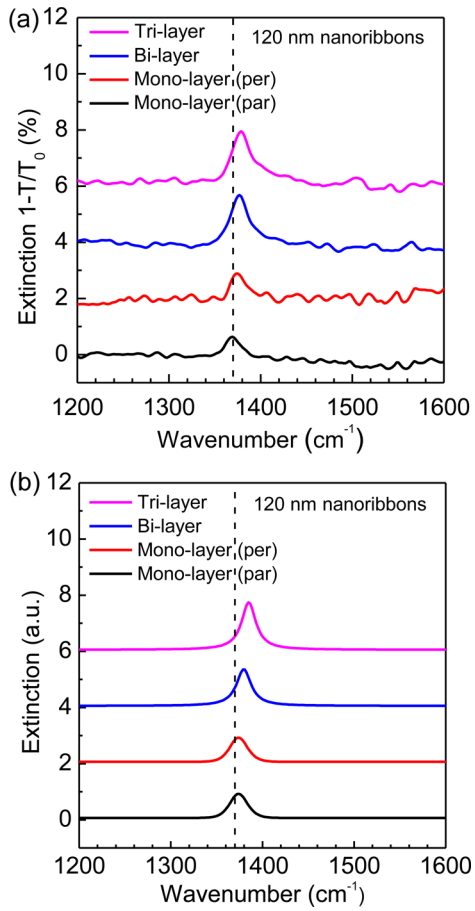

Figure 2. Phonon polaritons in hBN nanoribbons on SiO_2. (a) Measured extinction spectra of few-layer hBN nanoribbon arrays on SiO_2. Black curve is for monolayer hBN, with the incident light polarized parallel to the ribbons. The red, blue, and magenta curves are for mono-, bi-, and trilayer ribbon arrays, with the incident light polarized perpendicular to the ribbons. Spectra are consecutively shifted by 2% vertically for clarity. (b) Finite-difference time domain simulated extinction spectra of few-layer hBN nanoribbon arrays. Black curve is for monolayer hBN, with the incident light polarized parallel to the ribbons. The red, blue, and magenta curves are for mono-, bi-, and trilayer ribbon arrays with the incident light polarized perpendicular to the ribbons. Spectra are consecutively shifted vertically for clarity. In both (a) and (b), W_e = 120 nm. The dashed line indicates the Γ point phonon at 1370 cm^{-1}.

The phenomena above are manifestations of localized phonon polariton excitations due to the coupling between incident light and infrared-active hBN E_{1u} phonons.[35] These Fuchs−Kliewer optical phonons in the upper Reststrahlen band have a universal resonant frequency ω_Γ = 1370 cm^{-1} at the Γ point for arbitrary hBN thickness.[36] Away from the Γ point, the resonant frequency upshifts with dispersion, depending not only on in-plane wave vector $q_\perp$ but also on hBN thickness. Without in-plane boundary confinement, light polarized parallel to the ribbons has $q_\perp = 0$ and thus only couples to phonons at the Γ point, regardless of hBN thickness.[36] On the other hand, photons polarized perpendicular to the ribbons acquire nonvanishing $q_\perp \propto 1/W_e$ and result in excitations of phonons away from the Γ point with higher frequency than ω_Γ. Near the Γ point, the infrared-active phonons disperse more rapidly in thicker hBN due to the presence of long-range Coulomb interactions among layers. In general, for an N-layer hBN system, the E_{1u} phonon mode is N-fold degenerate at the Γ point. The degeneracy is lifted away from the Γ point, where multiple phonon branches emerge.[35] The observed phonon resonance in multilayer hBN corresponds to the excitation in the highest branch.[32] Finally, we attribute the increasing extinction intensity with hBN thickness to the rising phonon density (or the phonon oscillating strength); that is, more phonons are available to couple with incident photons in thicker hBN.

We performed a finite-difference time-domain (FDTD) simulation for light transmission through hBN nanoribbon arrays. In this simulation, the complex dielectric constant of hBN is extracted from a classical oscillator model.[25] Simulation details are presented in the Supporting Information. The results in Figure 2b reveal qualitative agreement with our experiment.

The tunable phonon properties of hBN in a layer-by-layer manner allow us to engineer the infrared response of graphene−hBN heterostructures. Figure 3 presents the measured extinction spectra for (a) graphene/hBN and (b) graphene/hBN/hBN heterostructure nanoribbon arrays with different W_e. In both cases, a monolayer graphene was first placed on the substrate followed by subsequent hBN layer transfers. Two eminent peaks in the spectral range around 1370 cm^{-1} stem from the long-range Fröhlich coupling between plasmons in graphene and polar phonons in hBN.[37] These two hybridized modes are characterized by the wave vector $q \simeq \pi/W_e$.[11] A common trend in both heterostructures is that the linewidth of the higher frequency peak narrows as its frequency approaches 1370 cm^{-1}, where it gains more phonon-like characteristics with extended lifetime.[38] As a result, the amplitude of this peak around 1370 cm^{-1} in graphene/hBN/hBN ribbons shows stronger extinction.

DOI: 10.1021/acsphotonics.5b00099
ACS Photonics 2015, 2, 907−912

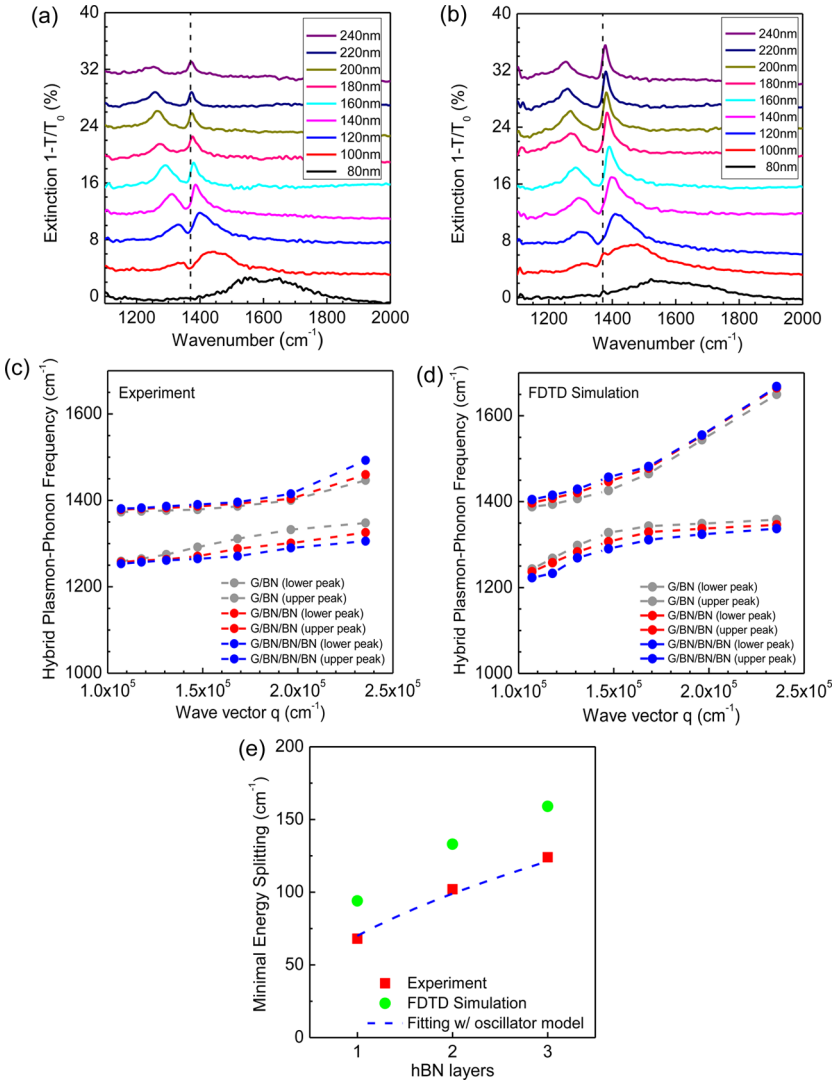

Figure 3. Plasmon−phonon polaritons in graphene/few-layer hBN heterostructure nanoribbons. (a,b) Infrared extinction spectra of graphene/hBN and graphene/hBN/hBN nanoribbon arrays on SiO_2. The incident light is always polarized perpendicular to the ribbons. W_e varies from 80 to 240 nm. Dashed line indicates the Γ point phonon at 1370 cm^{-1}. Spectra are shifted vertically by 4% consecutively for clarity. (c,d) Experimental and simulated plasmon−phonon polariton dispersions of heterostructures with a different number of hBN layers. Symbols represent experimental (c) and simulated (d) results. Dashed lines are for visualization only. (e) Dependence of minimal energy splitting on hBN thickness. Red squares (green circles) correspond to experimental (FDTD simulated) results extracted from panel c (panel d). Blue dashed line is a theoretic fit using $\sqrt{N}\Omega_s$ (Ω_s = 70 cm^{-1}). For details, see the Supporting Information.

Similar to vacuum Rabi splitting in optical semiconductor cavities,[39] the coupling strength of the plasmon−phonon polaritons is proportional to the minimal energy splitting between the hybrid modes. Figure 3c plots the experimental plasmon−phonon polariton dispersions for three different heterostructures with mono-, bi-, and trilayer hBN layers on top of a monolayer graphene. It is clearly shown that the graphene/hBN heterostructure has the weakest coupling strength, with a minimal splitting of 68 cm^{-1}, due to the low phonon density in a monolayer hBN. By contrast, the graphene/hBN/hBN/hBN heterostructure exhibits the strongest coupling strength with a minimal splitting of 124 cm^{-1}. Evidently, the coupling strength increases monotonically with growing hBN thickness. Figure 3d shows the calculated dispersion relations from FDTD simulations, which qualitatively agree with those obtained from experiments, albeit with larger coupling strength (i.e., 94 cm^{-1} for graphene/hBN, 133 cm^{-1} for graphene/hBN/hBN, and 159 cm^{-1} for graphene/hBN/hBN/hBN, respectively). Figure 3e presents the dependence of the minimal energy splitting on hBN thickness in both experiments and FDTD simulations. We attribute the slightly smaller splitting observed in experiments compared with simulations to the finite distance between adjacent layers introduced during layer transfer, which reduces the coupling strength of plasmon−phonon polaritons, while in the simulation, zero layer-to-layer spacing is assumed.

In the vicinity of the hBN phonon frequency, we notice a transparency window accompanied by asymmetric extinction line shape, implying a drastic variation of dielectric response.[40] Such phonon-induced transparency (PIT) phenomena result from the strong coupling between broadband plasmon excitations and discrete phonon oscillations,[41] which will interfere destructively if the graphene plasmon frequency is tuned to coincide with hBN phonon frequency, resulting in a sharp decrease in group velocity.[42] At the transparency, the

DOI: 10.1021/acsphotonics.5b00099
ACS Photonics 2015, 2, 907−912

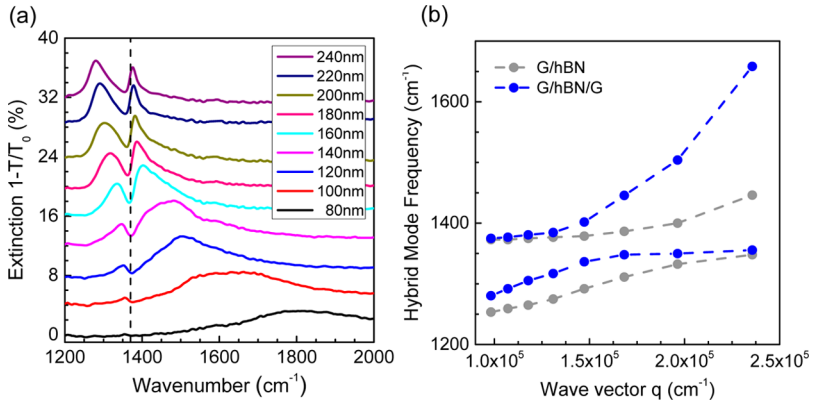

Figure 4. Plasmon−phonon polaritons in graphene/hBN/graphene heterostructure nanoribbons. (a) Extinction spectra of graphene/hBN/graphene heterostructure nanoribbon arrays on SiO_2. The incident light is always polarized perpendicular to the ribbons. W_e varies from 80 to 240 nm. Dashed line indicates the the Γ point phonon at 1370 cm^{-1}. Spectra are shifted vertically by 4% consecutively for clarity. (b) Plasmon−phonon polariton dispersions of nanoribbon arrays for graphene/hBN (gray) and graphene/hBN/graphene (blue) extracted from experimental extinction spectra. Symbols are experimental data. Dashed lines are for visualization.

group velocity can be written as (see Supporting Information for details)

$$v_g \approx \frac{5}{2}\frac{\Omega_s^2}{N\omega_\Gamma^2}c \quad (1)$$

where c is the speed of light in vacuum, N is the number of hBN layers, and Ω_s is the coupling energy associated with the strong coherent interaction between plasmons and phonons; $\Omega_s \approx 70$ cm^{-1} in our experiments (see Supporting Information for details). Equation 1 implies that the light group velocity is inversely proportional to hBN thickness as higher phonon density will add to the strength of the coupling. We emphasize that eq 1 is valid only for small N, where the penetration depth of the graphene plasmon field is much larger than the hBN thickness.[43] The penetration depth is limited to tens of nanometers due to the strong confinement of graphene plasmon field.[27] From eq 1, we conclude a slow light factor of 2870 (i.e., $v_g \approx c/2870$) for graphene/hBN/hBN/hBN. The slow group velocity is accompanied by an increased energy density as a result of the energy conservation law.[44] Therefore, a large amount of electromagnetic energy is stored within a few atomic layers, which may allow for the exploration of low-light-level nonlinear optics in mid-infrared.

By varying the thickness of hBN in a layer-by-layer manner, we demonstrate the tunability of coupling strength in the graphene−hBN heterostructure. However, the peak infrared extinction is limited by the relatively weak hBN phonon oscillating strength. Recall that the infrared extinction at the resonance peak of monolayer hBN is ∼0.7% (Figure 2a), much less than that of monolayer graphene plasmons in the same frequency range.[11] In order to enhance the extinction, we sandwich a monolayer hBN between two graphene layers to utilize the strong dipole−dipole coupling between top and bottom graphene plasmons. Figure 4a illustrates the extinction spectra for graphene/hBN/graphene nanoribbon arrays, in which the magnitudes of both peaks are greatly enhanced with a maximum exceeding 6% at W_e = 160 nm. Dipole−dipole coupling of plasmons between top and bottom graphene layer results in a significant increase of infrared absorption. Nevertheless, a comparison between the plasmon−phonon polariton dispersions of graphene/hBN and graphene/hBN/graphene in Figure 4b reveals that minimal energy splitting is barely altered. Much stronger plasmon oscillating strength in graphene/hBN/graphene heterostructure leads to higher polaritonic resonance frequencies (blue vs gray in Figure 4b). However, minimal splitting remains at ∼68 cm^{-1} in both cases. This further confirms that phonon oscillating strength in hBN dominates the degree of plasmon−phonon hybridization. By increasing graphene layers, we are able to enhance the infrared extinction of hybrid modes while maintaining the same coupling strength.

CONCLUSION

In summary, we demonstrate that the degree of plasmon−phonon hybridization and the overall plasmon oscillating strength in graphene−hBN heterostructures can be controlled simultaneously. The strong coupling between graphene plasmons and hBN phonons, and thus the accompanying slow light effect,[45−47] might inspire new experiments in nonlinear optics in the less-explored mid-infrared. PIT in our heterostructure devices demonstrates strong spectrum selectivity, which might be leveraged for optical filtering. Furthermore, the tunability of plasmon−phonon polaritons provides a new approach toward designing vertically stacked van der Waals heterostructures with extreme light confinement and tailored optical properties.

ASSOCIATED CONTENT

Supporting Information

Fabrication processes and numerical simulation procedures. The Supporting Information is available free of charge on the ACS Publications website at DOI: 10.1021/acsphotonics.5b00099.

AUTHOR INFORMATION

Corresponding Author

*E-mail: fengnian.xia@yale.edu.

Notes

The authors declare no competing financial interest.

ACKNOWLEDGMENTS

We acknowledge the support from the Office of Naval Research (N00014-14-1-0565).

DOI: 10.1021/acsphotonics.5b00099
ACS Photonics 2015, 2, 907−912

REFERENCES

(1) Chen, J.; Badioli, M.; Alonso-Gonzalez, P.; Thongrattanasiri, S.; Huth, F.; Osmond, J.; Spasenovic, M.; Centeno, A.; Pesquera, A.; Godignon, P.; Elorza, A. Z.; Camara, N.; Garcia de Abajo, F. J.; Hillenbrand, R.; Koppens, F. H. Optical nano-imaging of gate-tunable graphene plasmons. *Nature* **2012**, *487*, 77−81.

(2) Fei, Z.; Rodin, A. S.; Andreev, G. O.; Bao, W.; McLeod, A. S.; Wagner, M.; Zhang, L. M.; Zhao, Z.; Thiemens, M.; Dominguez, G.; Fogler, M. M.; Castro Neto, A. H.; Lau, C. N.; Keilmann, F.; Basov, D. N. Gate-tuning of graphene plasmons revealed by infrared nano-imaging. *Nature* **2012**, *487*, 82−85.

(3) Ju, L.; Geng, B.; Horng, J.; Girit, C.; Martin, M.; Hao, Z.; Bechtel, H. A.; Liang, X.; Zettl, A.; Shen, Y. R.; Wang, F. Graphene plasmonics for tunable terahertz metamaterials. *Nat. Nanotechnol.* **2011**, *6*, 630−634.

(4) Yan, H.; Li, X.; Chandra, B.; Tulevski, G.; Wu, Y.; Freitag, M.; Zhu, W.; Avouris, P.; Xia, F. Tunable infrared plasmonic devices using graphene/insulator stacks. *Nat. Nanotechnol.* **2012**, *7*, 330−334.

(5) Nikitin, A. Y.; Guinea, F.; Martin-Moreno, L. Resonant plasmonic effects in periodic graphene antidot arrays. *Appl. Phys. Lett.* **2012**, *101*, 151119.

(6) Liu, P.; Cai, W.; Wang, L.; Zhang, X.; Xu, J. Tunable terahertz optical antennas based on graphene ring structures. *Appl. Phys. Lett.* **2012**, *100*, 153111.

(7) Fang, Z.; Thongrattanasiri, S.; Schlather, A.; Liu, Z.; Ma, L.; Wang, Y.; Ajayan, P. M.; Nordlander, P.; Halas, N. J.; García de Abajo, F. J. Gated Tunability and Hybridization of Localized Plasmons in Nanostructured Graphene. *ACS Nano* **2013**, *7*, 2388−2395.

(8) Fei, Z.; Andreev, G. O.; Bao, W.; Zhang, L. M.; McLeod, A. S.; Wang, C.; Stewart, M. K.; Zhao, Z.; Dominguez, G.; Thiemens, M.; Fogler, M. M.; Tauber, M. J.; Castro-Neto, A. H.; Lau, C. N.; Keilmann, F.; Basov, D. N. Infrared nanoscopy of dirac plasmons at the graphene-SiO_2 interface. *Nano Lett.* **2011**, *11*, 4701−4705.

(9) Hill, A.; Mikhailov, S. A.; Ziegler, K. Dielectric function and plasmons in graphene. *Europhys. Lett.* **2009**, *87*, 27005.

(10) Fang, Z.; Wang, Y.; Schlather, A. E.; Liu, Z.; Ajayan, P. M.; Garcia de Abajo, F. J.; Nordlander, P.; Zhu, X.; Halas, N. J. Active tunable absorption enhancement with graphene nanodisk arrays. *Nano Lett.* **2014**, *14*, 299−304.

(11) Yan, H.; Low, T.; Zhu, W.; Wu, Y.; Freitag, M.; Li, X.; Guinea, F.; Avouris, P.; Xia, F. Damping pathways of mid-infrared plasmons in graphene nanostructures. *Nat. Photonics* **2013**, *7*, 394−399.

(12) Jablan, M.; Buljan, H.; Soljačić, M. Plasmonics in graphene at infrared frequencies. *Phys. Rev. B: Condens. Matter Mater. Phys.* **2009**, *80*, 245435.

(13) Cai, X.; Sushkov, A. B.; Suess, R. J.; Jadidi, M. M.; Jenkins, G. S.; Nyakiti, L. O.; Myers-Ward, R. L.; Li, S.; Yan, J.; Gaskill, D. K.; Murphy, T. E.; Drew, H. D.; Fuhrer, M. S. Sensitive room-temperature terahertz detection via the photothermoelectric effect in graphene. *Nat. Nanotechnol.* **2014**, *9*, 814−819.

(14) Freitag, M.; Low, T.; Zhu, W.; Yan, H.; Xia, F.; Avouris, P. Photocurrent in graphene harnessed by tunable intrinsic plasmons. *Nat. Commun.* **2013**, *4*, 1951.

(15) Grigorenko, A. N.; Polini, M.; Novoselov, K. S. Graphene plasmonics. *Nat. Photonics* **2012**, *6*, 749−758.

(16) Li, Y.; Yan, H.; Farmer, D. B.; Meng, X.; Zhu, W.; Osgood, R. M.; Heinz, T. F.; Avouris, P. Graphene plasmon enhanced vibrational sensing of surface-adsorbed layers. *Nano Lett.* **2014**, *14*, 1573−1577.

(17) Xia, F.; Yan, H.; Avouris, P. The Interaction of Light and Graphene: Basics, Devices, and Applications. *Proc. IEEE* **2013**, *101*, 1717−1731.

(18) Christensen, J.; Manjavacas, A.; Thongrattanasiri, S.; Koppens, F. H. L.; García de Abajo, F. J. Graphene Plasmon Waveguiding and Hybridization in Individual and Paired Nanoribbons. *ACS Nano* **2012**, *6*, 431−440.

(19) Liu, R.; Fu, X. W.; Meng, J.; Bie, Y. Q.; Yu, D. P.; Liao, Z. M. Graphene plasmon enhanced photoluminescence in ZnO microwires. *Nanoscale* **2013**, *5*, 5294−5298.

(20) Bao, Q.; Loh, K. P. Graphene Photonics, Plasmonics, and Broadband Optoelectronic Devices. *ACS Nano* **2012**, *6*, 3677−3694.

(21) Link, S.; El-Sayed, M. A. Spectral Properties and Relaxation Dynamics of Surface Plasmon Electronic Oscillations in Gold and Silver Nanodots and Nanorods. *J. Phys. Chem. B* **1999**, *103*, 8410−8426.

(22) García de Abajo, F. J. Graphene Plasmonics: Challenges and Opportunities. *ACS Photonics* **2014**, *1*, 135−152.

(23) Castro Neto, A. H.; Peres, N. M. R.; Novoselov, K. S.; Geim, A. K. The electronic properties of graphene. *Rev. Mod. Phys.* **2009**, *81*, 109−162.

(24) Manjavacas, A.; Liu, J. G.; Kulkarni, V.; Nordlander, P. Plasmon-Induced Hot Carriers in Metallic Nanoparticles. *ACS Nano* **2014**, *8*, 7630−7638.

(25) Geick, R.; Perry, C.; Rupprecht, G. Normal Modes in Hexagonal Boron Nitride. *Phys. Rev.* **1966**, *146*, 543−547.

(26) Oshima, C.; Nagashima, A. Ultra-thin epitaxial films of graphite and hexagonal boron nitride on solid surfaces. *J. Phys.: Condens. Matter* **1997**, *9*, 1−21.

(27) Brar, V. W.; Jang, M. S.; Sherrott, M.; Kim, S.; Lopez, J. J.; Kim, L. B.; Choi, M.; Atwater, H. Hybrid surface-phonon-plasmon polariton modes in graphene/monolayer h-BN heterostructures. *Nano Lett.* **2014**, *14*, 3876−3880.

(28) Dai, S.; Ma, Q.; Zhu, S.-E.; Liu, M. K.; Andersen, T.; Fei, Z.; Goldflam, M.; Wagner, M.; Watanabe, K.; Taniguchi, T.; Thiemens, M.; Keilmann, F.; Janssen, G. C. A. M.; Jarillo-Herrero, P.; Fogler, M. M.; Basov, D. N. Graphene on hexagonal boron nitride as an agile hyperbolic metamaterial. *Nat. Nanotechnol.* **2015**, DOI: 10.1038/nnano.2015.131.

(29) Li, X.; Cai, W.; An, J.; Kim, S.; Nah, J.; Yang, D.; Piner, R.; Velamakanni, A.; Jung, I.; Tutuc, E.; Banerjee, S. K.; Colombo, L.; Ruoff, R. S. Large-area synthesis of high-quality and uniform graphene films on copper foils. *Science* **2009**, *324*, 1312−1314.

(30) Geim, A. K.; Grigorieva, I. V. Van der Waals heterostructures. *Nature* **2013**, *499*, 419−425.

(31) Tinkham, M. Energy Gap Interpretation of Experiments on Infrared Transmission through Superconducting Films. *Phys. Rev.* **1956**, *104*, 845−846.

(32) Dai, S.; Fei, Z.; Ma, Q.; Rodin, A. S.; Wagner, M.; McLeod, A. S.; Liu, M. K.; Gannett, W.; Regan, W.; Watanabe, K.; Taniguchi, T.; Thiemens, M.; Dominguez, G.; Castro Neto, A. H.; Zettl, A.; Keilmann, F.; Jarillo-Herrero, P.; Fogler, M. M.; Basov, D. N. Tunable phonon polaritons in atomically thin van der Waals crystals of boron nitride. *Science* **2014**, *343*, 1125−1129.

(33) Garcia-Pomar, J. L.; Nikitin, A. Y.; Martin-Moreno, L. Scattering of Graphene Plasmons by Defects in the Graphene Sheet. *ACS Nano* **2013**, *7*, 4988−4994.

(34) Caldwell, J. D.; Kretinin, A. V.; Chen, Y.; Giannini, V.; Fogler, M. M.; Francescato, Y.; Ellis, C. T.; Tischler, J. G.; Woods, C. R.; Giles, A. J.; Hong, M.; Watanabe, K.; Taniguchi, T.; Maier, S. A.; Novoselov, K. S. Sub-diffractional volume-confined polaritons in the natural hyperbolic material hexagonal boron nitride. *Nat. Commun.* **2014**, *5*, 5221.

(35) Michel, K. H.; Verberck, B. Phonon dispersions and piezoelectricity in bulk and multilayers of hexagonal boron nitride. *Phys. Rev. B: Condens. Matter Mater. Phys.* **2011**, *83*, 115328.

(36) Fuchs, R.; Kliewer, K. Optical Modes of Vibration in an Ionic Crystal Slab. *Phys. Rev.* **1965**, *140*, A2076−A2088.

(37) Hwang, E. H.; Sensarma, R.; Das Sarma, S. Plasmon−phonon coupling in graphene. *Phys. Rev. B: Condens. Matter Mater. Phys.* **2010**, *82*, 195406.

(38) Low, T.; Avouris, P. Graphene Plasmonics for Terahertz to Mid-Infrared Applications. *ACS Nano* **2014**, *8*, 1086−1101.

(39) Khitrova, G.; Gibbs, H. M.; Kira, M.; Koch, S. W.; Scherer, A. Vacuum Rabi splitting in semiconductors. *Nat. Phys.* **2006**, *2*, 81−90.

(40) Hau, L. V.; Harris, S. E.; Dutton, Z.; Behroozi, C. H. Light speed reduction to 17 metres per second in an ultracold atomic gas. *Nature* **1999**, *397*, 594−598.

DOI: 10.1021/acsphotonics.5b00099
ACS Photonics 2015, 2, 907−912

(41) Luk'yanchuk, B.; Zheludev, N. I.; Maier, S. A.; Halas, N. J.; Nordlander, P.; Giessen, H.; Chong, C. T. The Fano resonance in plasmonic nanostructures and metamaterials. *Nat. Mater.* **2010**, *9*, 707−715.
(42) Yan, H.; Low, T.; Guinea, F.; Xia, F.; Avouris, P. Tunable phonon-induced transparency in bilayer graphene nanoribbons. *Nano Lett.* **2014**, *14*, 4581−4586.
(43) Woessner, A.; Lundeberg, M. B.; Gao, Y.; Principi, A.; Alonso-Gonzalez, P.; Carrega, M.; Watanabe, K.; Taniguchi, T.; Vignale, G.; Polini, M.; Hone, J.; Hillenbrand, R.; Koppens, F. H. Highly confined low-loss plasmons in graphene-boron nitride heterostructures. *Nat. Mater.* **2015**, *14*, 421−425.
(44) Kasapi, A.; Jain, M.; Yin, G.; Harris, S. Electromagnetically Induced Transparency: Propagation Dynamics. *Phys. Rev. Lett.* **1995**, *74*, 2447−2450.
(45) Xia, F.; Mueller, T.; Lin, Y. M.; Valdes-Garcia, A.; Avouris, P. Ultrafast graphene photodetector. *Nat. Nanotechnol.* **2009**, *4*, 839−43.
(46) Cox, J. D.; Javier Garcia de Abajo, F. Electrically tunable nonlinear plasmonics in graphene nanoislands. *Nat. Commun.* **2014**, *5*, 5725.
(47) Tucker, R.; Ku, P.-C.; Chang-Hasnain, C. J. Slow-light optical buffers: capabilities and fundamental limitations. *J. Lightwave Technol.* **2005**, *23*, 4046−4066.

DOI: 10.1021/acsphotonics.5b00099
ACS Photonics 2015, 2, 907−912